

VLES Study of Ship Stack Gas Dynamics

F. Camelli, R. Löhner
School of Computational Sciences
Laboratory for Computational Fluid Dynamics
George Mason University, M.S. 4C7
Fairfax, VA 22030-4444, e-mail:fcamelli@gmu.edu

W.C. Sandberg, and R. Ramamurti
Laboratory for Computational Physics and Fluid Dynamics
Naval Research Laboratory
Washington, DC 20375-5344

Abstract

The present paper presents the results of the numerical study of the stack gas temperature field and the levels of concentration of different species around the new surface vessel T-AKE 1. A VLES simulation of the flow was performed using a Smagorinsky turbulence closure model. The time integration was done with a multi-stage explicit advective prediction scheme for projection-type incompressible solvers. The study was performed for a 0° and 30° angle of attack inflow. The computed results for the temperature and concentration agree well with the experimental data.

1 Introduction

In the course of evaluating alternative design concepts and also the analysis of ship performance for a selected configuration, computational assessments are a necessity. There is neither the time nor the funds to experimentally evaluate all design alternatives for all operational requirements. A very attractive option that can bridge the need for more detailed and fast information is the collaborative use of experimental information, e.g. wind tunnel and virtual experiments, in particular computational fluid dynamics (CFD). However, it is necessary to validate the numerical tools first in order to accept this additional information as reliable and accurate. An important issue of accepting numerical experiments is that they must provide a physical model that is realistic enough to represent the problem. We devote the present study to the performance assessment of a selected stack design configuration as distinct from other issues associated with topside design. The stack design technology is reviewed in [2]. Most of the interest on this area has been in naval vessels. The two main issues in the stack design are tem-

perature and concentration levels. Temperature in the outlet of the stacks usually rises to 300°C , producing a distinctive signature that is not desirable in naval vessels. Many times the hot gasses and particulates from the stacks are trapped in the recirculation zones and therefore the concentration levels of species like SO_2 , NO_x , or CO rise above healthy levels, putting the crew and the ship at risk. The gas jet from the stacks is an unsteady phenomena and it needs to be treated in this way. Many numerical approaches developed in the past rely on statistics and therefore miss the transient characteristics of the problem. In order to capture the unsteadiness of the problem, a very large eddy simulation (VLES) was used. There have been a number of computational studies of ship topside airwake recently [20, 24, 10, 9, 22, 23, 14]. We have carried out computational airwake studies which addressed helo landing [15], and stack gas flow and ingestion into ship spaces [6, 16, 17]. The present study includes the coupling of the ship topside flow to the thermal transport and diffusion of the gas from multiple stacks. The present study addresses the case for 0° and 30° angle of attack of the inflow.

2 Time Integration Scheme

We use an explicit integration in time for the advective terms in order to capture the unsteadiness of the flow around the superstructure of the T-AKE 1. Most of the diffusion in the atmosphere is due to the turbulent nature of the flow. The molecular diffusion is usually two orders of magnitude lower than the turbulent diffusion. Therefore, the time step selected for integration in time has to be small enough such that it is possible to capture all the high frequencies that contribute to the turbulent diffusion.

2.1 Projection Scheme

The equations describing incompressible, Newtonian flows are written as

$$\mathbf{v}_{,t} + \mathbf{v}\nabla\mathbf{v} + \nabla p = \nabla\mu\nabla\mathbf{v}, \quad (1)$$

$$\nabla\mathbf{v} = 0 \quad (2)$$

Here p denotes the pressure, \mathbf{v} the velocity vector and both the pressure p and the viscosity have been normalized by the (constant) density ρ . The important physical phenomena propagate with the advective timescales, i.e. with \mathbf{v} . Diffusive phenomena typically occur at a much faster rate, and can/should therefore be integrated implicitly. Given that the pressure establishes itself immediately through the pressure-Poisson equation, an implicit integration of pressure is also required. The hyperbolic character of the advection operator and the elliptic character of the pressure-Poisson equation have led to a number of so-called projection schemes. The key idea is to predict first a velocity field from the current flow variables without taking the divergence constraint into account. In a second step, the divergence constraint is separated into an advective-diffusive and pressure increment:

$$\mathbf{v}^{n+1} = \mathbf{v}^n + \Delta\mathbf{v}^a + \Delta\mathbf{v}^p = \mathbf{v}^* + \Delta\mathbf{v}^p. \quad (3)$$

For an explicit integration of the advective terms (with implicit integration of the viscous terms), one complete timestep is given by:

- Advective-Diffusive Prediction: $\mathbf{v}^n \rightarrow \mathbf{v}^*$

$$\left[\frac{1}{\Delta t} - \theta\nabla\mu\nabla \right] (\mathbf{v}^* - \mathbf{v}^n) + \mathbf{v}^n \cdot \nabla\mathbf{v}^n + \nabla p^n = \nabla\mu\nabla\mathbf{v}^n; \quad (4)$$

- Pressure Correction: $p^n \rightarrow p^{n+1}$

$$\nabla \cdot \mathbf{v}^{n+1} = 0; \quad (5)$$

$$\frac{\mathbf{v}^{n+1} - \mathbf{v}^*}{\Delta t} + \nabla (p^{n+1} - p^n) = 0; \quad (6)$$

which results in

$$\nabla^2 (p^{n+1} - p^n) = \frac{\nabla \cdot \mathbf{v}^*}{\Delta t}; \quad (7)$$

- Velocity Correction: $\mathbf{v}^* \rightarrow \mathbf{v}^{n+1}$

$$\mathbf{v}^{n+1} = \mathbf{v}^* - \Delta t \nabla (p^{n+1} - p^n). \quad (8)$$

At steady state, $\mathbf{v}^* = \mathbf{v}^n = \mathbf{v}^{n+1}$ and the residuals of the pressure correction vanish, implying that the results do not depend on the timestep Δt . θ denotes the implicitness-factor for the viscous terms ($\theta = 1$: 1st order, fully implicit, $\theta = 0.5$: 2nd order, Crank-Nicholson). This scheme has been widely used in conjunction with spatial discretization based on finite differences [13, 4, 5, 1], finite volumes [11], and finite elements [18, 21, 19, 8, 12].

2.2 Multi-stage Explicit Advective Prediction Scheme

The scheme given by Eqns.(4-8) is, at best, of 2nd order in time. It is surprising to note that apparently no attempt has been made to use multistage explicit schemes to integrate the advective terms with higher order or to accelerate the convergence to steady state. This may stem from the fact that the implicit integration of viscous terms apparently impedes taking the full advantage multistage schemes offer for the Euler limit of no viscosity. An interesting alternative, used here, is to integrate with different timestepping schemes in the different regimes of flows with highly variable cell Reynolds-number

$$Re_h = \frac{\rho\|\mathbf{v}\|h}{\mu}. \quad (9)$$

For the case $Re_h < 1$ (viscous dominated), the accuracy in time for the advective term is not so important. However, for $Re_h > 1$ (advection dominated), the advantages

of higher order time-marching schemes are considerable, particularly if one considers vortex transport over large distances. Dahlquist's theorem states that no unconditionally stable (implicit) scheme can be of order higher than two (this being the Cranck-Nicholson scheme). However, explicit schemes of the Runge-Kutta type can easily yield higher order timestepping. A k -step, time-accurate Runge-Kutta scheme for the advective parts may be written as:

$$\begin{aligned} \mathbf{v}^i &= \mathbf{v}^0 + \\ \alpha^i \gamma \Delta t (-\mathbf{v}^{i-1} \cdot \nabla \mathbf{v}^{i-1} - \nabla p^n + \nabla \mu \nabla \mathbf{v}^{i-1}) ; \\ i &= 1, k-1 ; \end{aligned} \quad (10)$$

$$\begin{aligned} \left[\frac{1}{\Delta t} - \theta \nabla \mu \nabla \right] (\mathbf{v}^k - \mathbf{v}^n) + \\ \mathbf{v}^{k-1} \cdot \nabla \mathbf{v}^{k-1} + \nabla p^n = \\ \nabla \mu \nabla \mathbf{v}^{k-1} . \end{aligned} \quad (11)$$

Here, the α^i are the standard Runge-Kutta coefficients, and θ is the implicitness-factor for the viscous terms ($\theta = 1$: 1st order, fully implicit, $\theta = 0.5$: 2nd order, Crank-Nicholson). The factor γ denotes the local ratio of the stability limit for explicit timestepping for the viscous terms versus the timestep chosen. Given that the advective and viscous timestep limits are proportional to:

$$\Delta t_a \approx \frac{h}{\|\mathbf{v}\|} ; \Delta t_v \approx \frac{\rho h^2}{\mu} , \quad (12)$$

we immediately obtain

$$\gamma = \frac{\Delta t_v}{\Delta t_a} \approx \frac{\rho \|\mathbf{v}\| h}{\mu} \approx Re_h . \quad (13)$$

In regions away from boundary layers, this factor is $O(1)$, implying that a high-order Runge-Kutta scheme is recovered. Note that not using γ leads to schemes that are not of second order for the advective terms, unless an unsymmetric matrix is allowed on the left hand side. Besides higher accuracy, an important benefit of explicit multi-stage advection schemes is the larger timestep one can employ. The increase in allowable timestep is roughly proportional to the stages used. Given that most of the CPU time is spent solving the pressure-Poisson system (5), the speedup achieved is also roughly proportional to the stages used.

3 Problem Description

The geometry of the T-AKE 1 is presented in Figure (1). The dimensions of the ship are: 210 m in length, 32 m in width, and 42 m in height above the waterline.

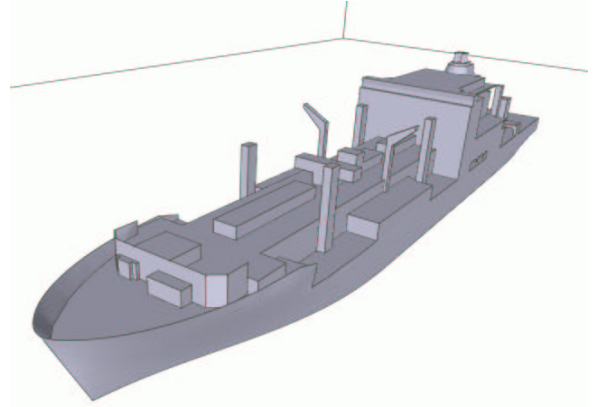


Figure 1: T-AKE 1.

An initial critical and time consuming step that must be taken before any computations is the generation of a 3-D surface model that accurately represents the ship and is suitable for CFD computations. The geometry recovery of the ship was made from different type of CAD files, and in several steps. First, the hull was recovered from IGES files, second the main deck and bridge from AutoCad 3-D files, third the bow part of the ship from AutoCad 2-D files, and finally the stack casing from AutoCad 2-D files. The stack casing is modeled with five pipes, four from the engines and one from the incinerator. Figures (2) to (5) show the different steps of the geometry definition. Figure (6) shows the final surface mesh of the T-AKE 1. The final volume mesh has 1,360,000 points and 7,600,000 tetrahedra.

The T-AKE is a transport ship with a cargo loading area in the bow and a helicopter landing pad in the stern. In the past, some naval transport ships have experienced problems with uncomfortable odors from the stack gas emission. In addition, the particulates emitted from the stacks can be a problem for the instruments, weapons, and sensitive parts of the vessel. We concentrated our temperature and concentration study for the 0° and 30° angle of attack with a ship speed of 14 knots (7.2 m/s) and a wind velocity of 24.5 knots (12.6 m/s) in both cases. The effects of hot gas were modeled with the Boussinesq's approximation for buoyancy.

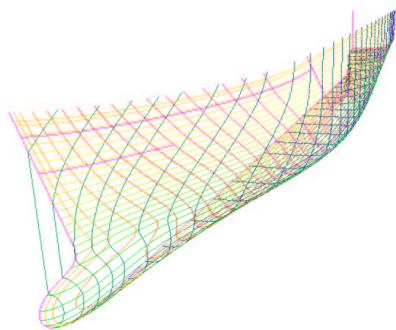


Figure 2: T-AKE 1 Hull - IGES File.

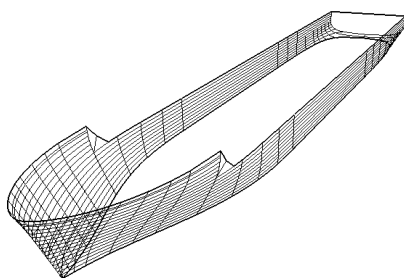


Figure 3: T-AKE 1 Hull - FECD File.

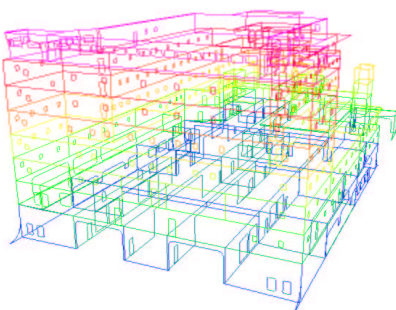


Figure 4: T-AKE 1 Bridge and Main Decks - IGES File.

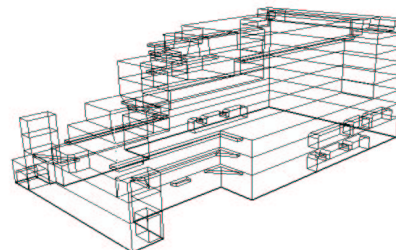


Figure 5: T-AKE 1 Bridge and Main Decks - FECD File.

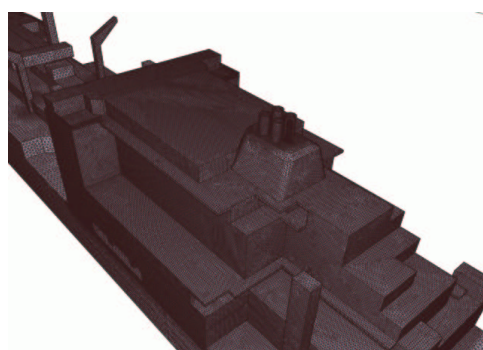


Figure 6: T-AKE 1 Surface Mesh - Close View.

4 Results

A VLES simulation was performed with the multi-stage explicit advective prediction scheme. The density was 1.225 kg/m^3 , and the viscosity was $1.789 \times 10^{-5} \text{ kg/m/s}$. The Reynolds number based on the height of the ship is 5×10^7 . The Law of the Wall was used for the wall boundary condition. The Smagorinsky turbulence model [25] was used. The unsteady characteristic of the flow around the vessel superstructure demands a time integration that preserves the high frequency modes and a fine resolution in the spatial mesh. A Courant number of $C = 1.0$ was used in the time integration in combination with 5 stages of Runge-Kutta. The timestep is approximately $\Delta t = 0.33 \times 10^{-2} \text{ s}$ which permits the capture of most of the high frequencies that are responsible for the diffusion of the gases. The solution was integrated for 2 minutes of real time on an SGI 3800 shared memory machine at the Naval Research Laboratory. This run required a month of computing time on 32 processors.

4.1 Case 0°

Snapshots of the velocity vectors and velocity contour lines in a cut plane are shown in Figures (7) and (8). The velocity vectors shows large regions of recirculation and a very complicated flow pattern above the landing deck.

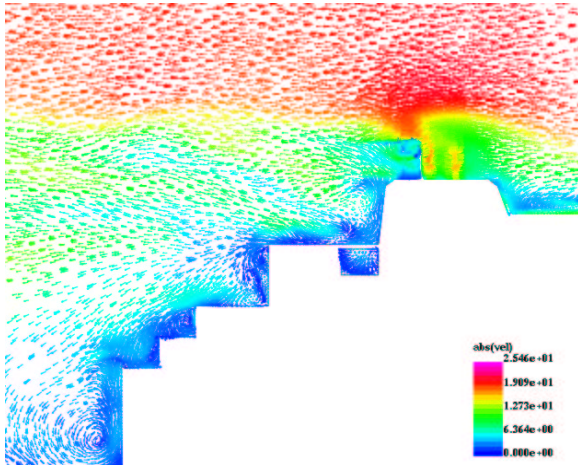


Figure 7: Velocity vectors (m/s) - 0° case.

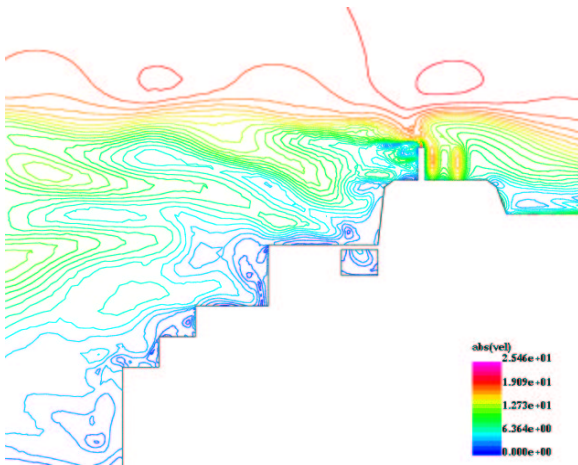


Figure 8: Velocity contour lines (m/s) - 0° case.

Two different techniques of visualization were applied to give a better understanding of the flow pattern. First, ribbons were used to visualize the flow. Figure (9) shows a large recirculation above the landing deck. The ribbons are instantaneous stream lines of the flow [3]. This technique helps to visually capture the areas with recirculation. To visualize more clearly the time-varying trajectory of the gas and impingement zones on the structure, particles colored with temperature were released from the stacks. Figure (10) shows one such snapshot of released particles.

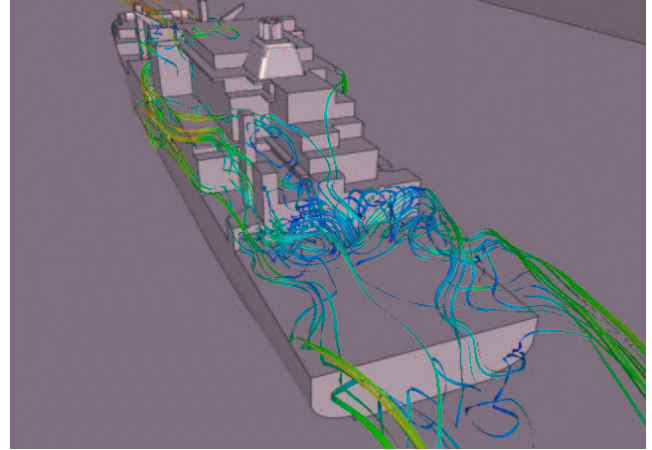


Figure 9: Instantaneous ribbons - 0° case.

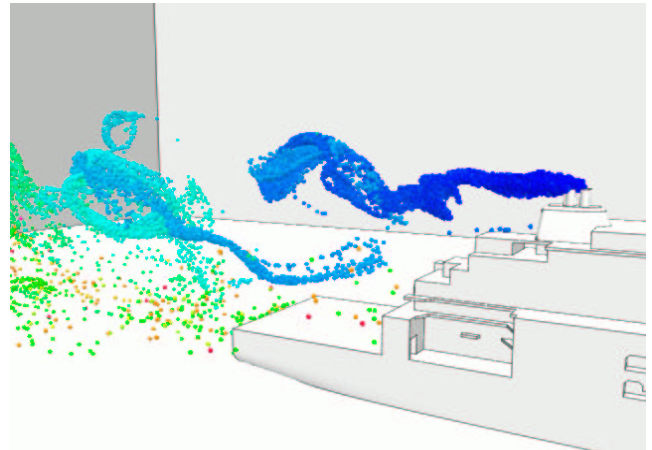


Figure 10: Release of particles from the stacks - 0° case.

4.1.1 Topside Concentration and Temperature Study

The flow simulation was coupled with the transport and diffusion of temperature and the transport and diffusion of two passive scalars. The scalars represent sulfur dioxide (SO_2) and nitric oxides (NO_x). An extensive series of wind tunnel experiments for the temperature and concentration levels were previously conducted by the Danish Maritime Institute (DMI) [7], hence data is available for comparison.

Table 1 summarizes the comparison of the computational results with the experimental data for the temperature. Tables 2 and 3 show the levels of concentration for three different positions. The positions where the temperature and concentration levels were taken are shown in Figure (11). The computational results were averaged

on a window time of 120 seconds. Figures (12) to (19) show the time histories for those points where the temperature and concentration levels were averaged.

Position	T _{exp} [°C]	T _{comp} [°C]	% diff
7	20.10	20.14	0.2
8	20.10	20.23	0.6
9	20.30	20.50	1.0
10	21.10	21.38	1.3
11	22.50	23.38	3.9

Table 1: Temperature Levels.

Position	c _{exp} [ppm]	c _{comp} [ppm]	% diff
1	0.1	0.086	14
2	0.2	0.156	22
4	0.0	0.000	0

Table 2: SO₂ Concentration Levels.

Position	c _{exp} [ppm]	c _{comp} [ppm]	% diff
1	0.6	0.396	34
2	0.7	0.716	2
4	0.0	0.000	0

Table 3: NO_x Concentration Levels.

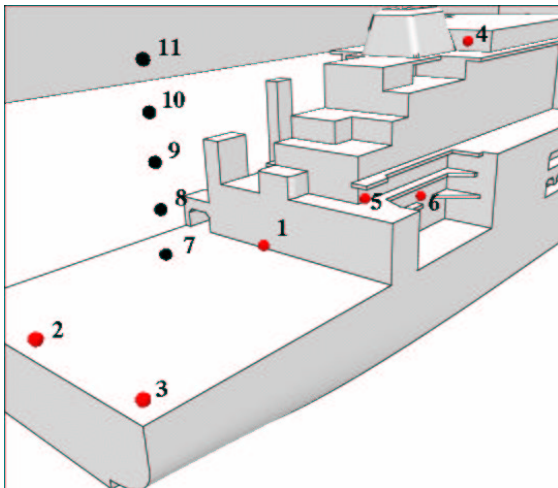


Figure 11: Position of stations.

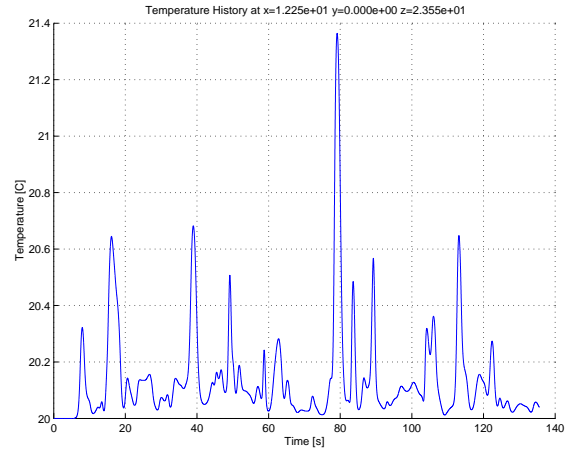


Figure 12: Temperature Time History at Position 7.

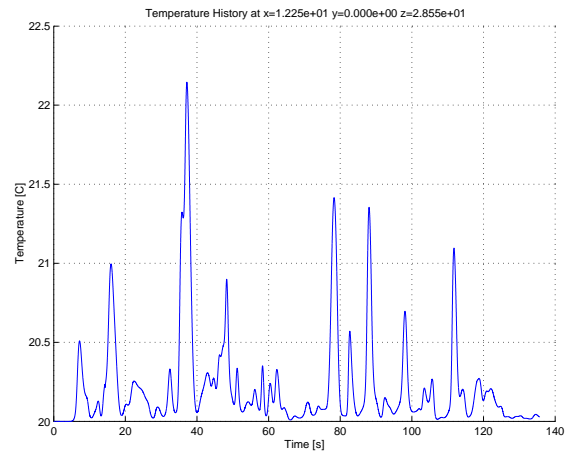


Figure 13: Temperature Time History at Position 8.

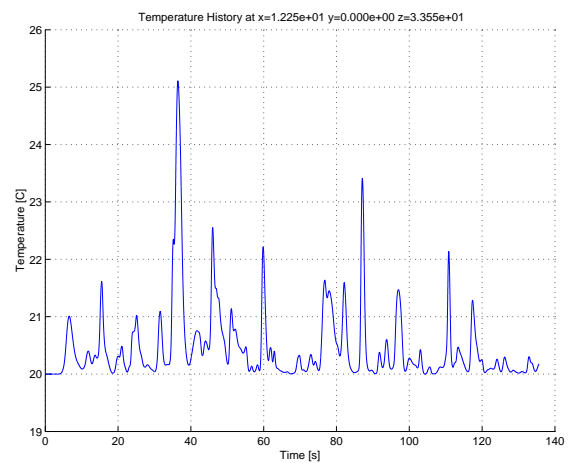


Figure 14: Temperature Time History at Position 9.

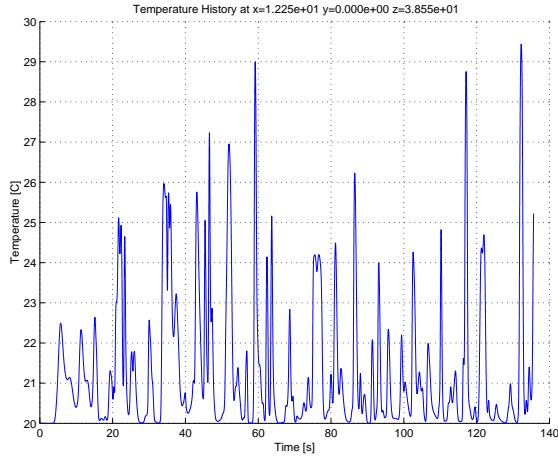


Figure 15: Temperature Time History at Position 10.

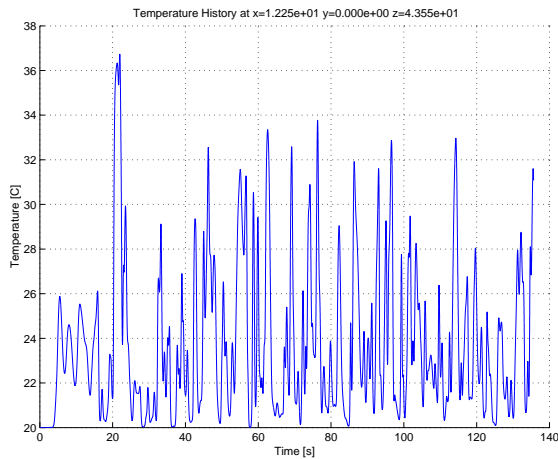


Figure 16: Temperature Time History at Position 11.

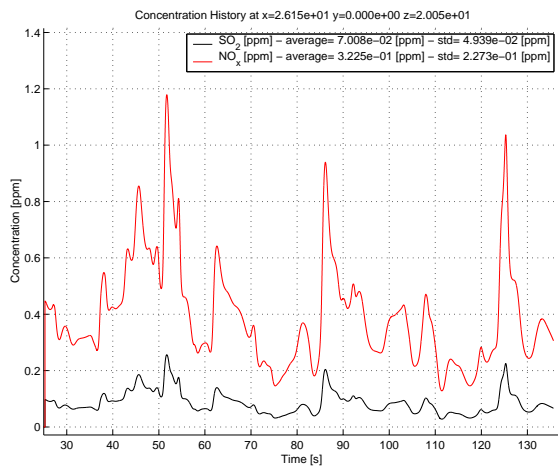


Figure 17: Concentration Time History at Position 1.

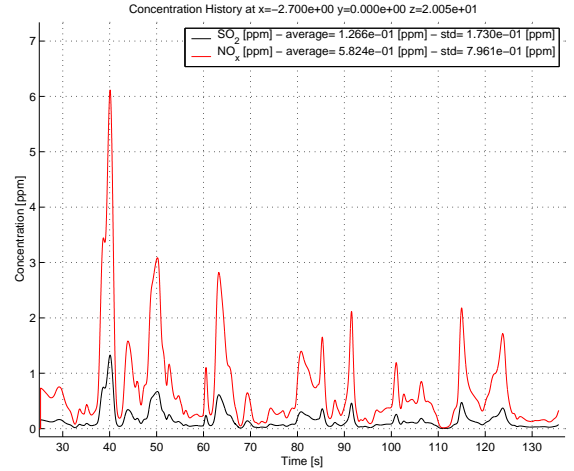


Figure 18: Concentration Time History at Position 2.

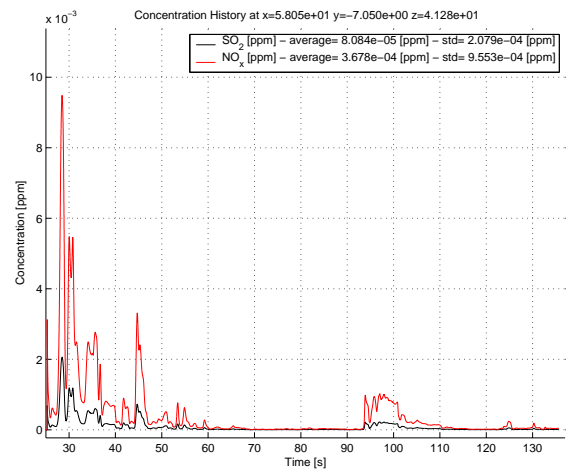


Figure 19: Concentration Time History at Position 4.

4.2 Case 30°

A cut plane of the absolute velocity is shown in Figure (20). Large zones of recirculation can be observed in the landing deck. This correspond to a snapshot in time. Figure (22) shows particles colored with residence time, dark blue represents the new particles in the flow and magenta represents the oldest particles. Some particles remain for prolonged time in the starboard of the vessel, suggesting the existence of a large recirculation zone.

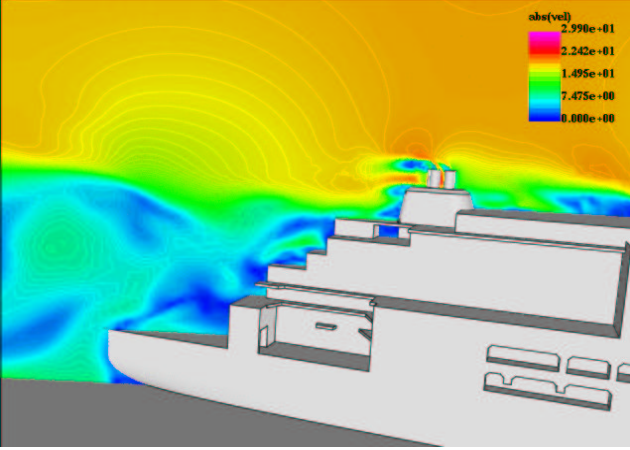


Figure 20: Contours of absolute velocity (m/s) - 30° case.

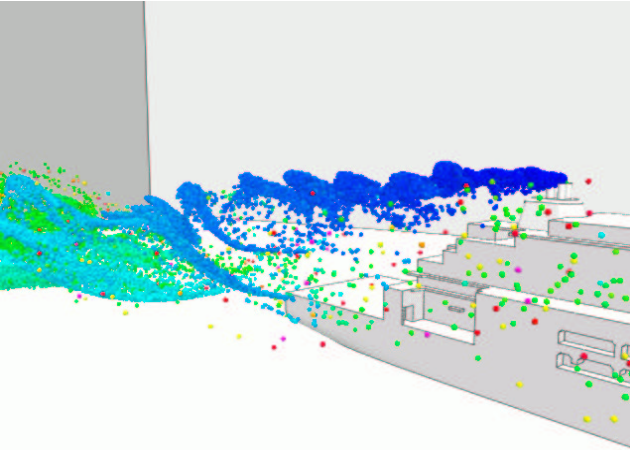


Figure 21: Release of particles from the stacks - 30° case.

4.2.1 Topside Concentration Study

The computed concentration levels for the SO₂ and NO_x are presented in Tables 4 and 5. Note that the experimental level of concentration for SO₂ is zero in stations 3 and 6, and the experimental level of concentration for NO_x is zero in station 6. The other computed levels agree well with the experiemntal values reported from DMI. Figures (22) to (24) show the time history for the concenmtration levels in the mentioned stations. Again, these graphs depict a highly turbulent behavior.

Position	c _{exp} [ppm]	c _{comp} [ppm]	% diff
3	0.0	0.057	—
5	0.1	0.089	11
6	0.0	0.039	—

Table 4: SO₂ Concentration Levels.

Position	c _{exp} [ppm]	c _{comp} [ppm]	% diff
3	0.2	0.262	31
5	0.5	0.410	18
6	0.0	0.183	—

Table 5: NO_x Concentration Levels.

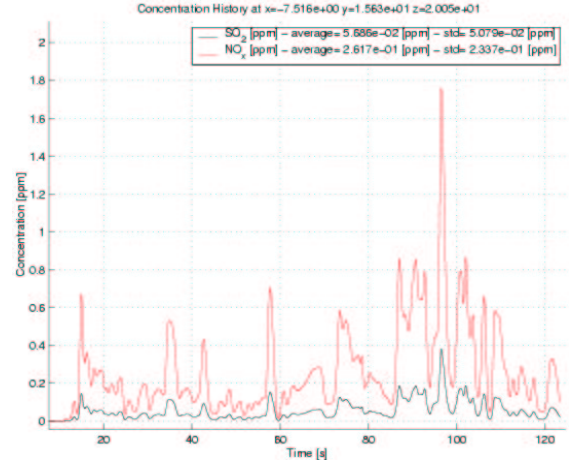


Figure 22: Concentration Time History at Position 3.

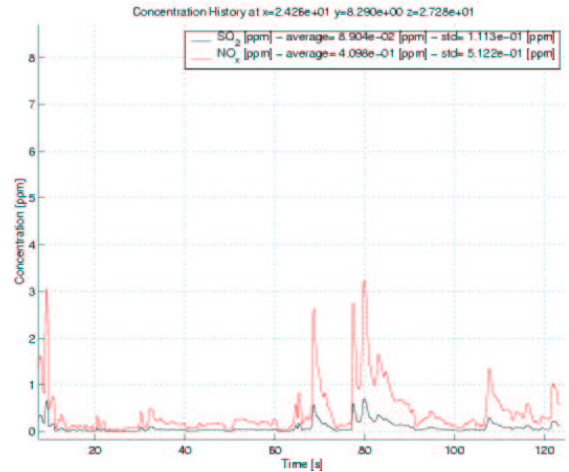


Figure 23: Concentration Time History at Position 5.

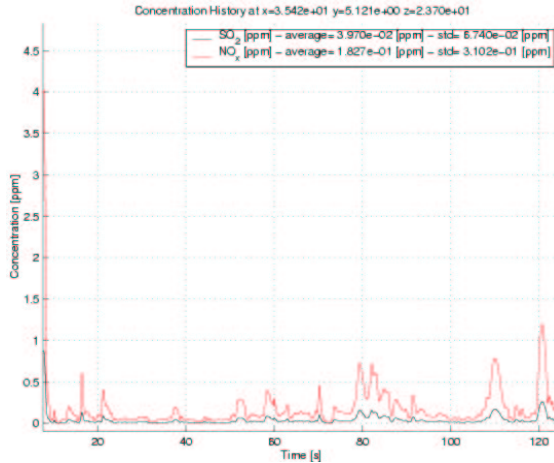


Figure 24: Concentration Time History at Position 9.

5 Discussion and Outlook

The multistage Runge-Kutta scheme was shown to provide a reduction in CPU time of the order of 10, preserving accuracy in the computational results. This gain in performance positions the explicit integration in a very competitive situation in comparison to implicit integration when the difference between both timesteps is not larger than two orders of magnitude. The numerical results for the temperature and concentration levels agree well with the experimental results from the wind tunnel study performed at DMI.

References

- [1] B. Alessandrini and G. Delhommeau. A multigrid velocity-pressure-free surface elevation fully coupled solver for calculation of turbulent incompressible flow around a hull. In *Proc. 21st Symp. on Naval Hydrodynamics*, Trondheim, Norway, June 1996.
- [2] G. J. Baham and D. MaCallum. Stack design technology for naval and merchant ships. *SNAME Transactions*, 85:324–349, 1977.
- [3] G. K. Batchelor. *An introduction to fluid dynamics*. Cambridge: University Press, reprinted paperback edition, 1983.
- [4] J. B. Bell, P. Colella, and H. Glaz. A second order projection method for the Navier-Stokes equations. *Journal of Computational Physics*, 85:257–283, 1989.
- [5] J. B. Bell and D. L. Marcus. A second order projection method for variable density flows. *Journal of Computational Physics*, 101, 1992.
- [6] F. Camelli, O. Soto, R. Löhner, W. C. Sandberg, and R. Ramamurti. Topside LPD17 flow and temperature study with an implicit monolithic scheme. *AIAA Paper 2003-0969*, 2003.
- [7] DMI. Wind-tunnel tests with T-AKE 1. Report 2002031, Danish Maritime Institute, June 2002.
- [8] E. Eaton. Aero-acoustic in an automotive HVAC module. In *American PAM User Conf.*, Birmingham, Michigan, October 2001.
- [9] M. J. Guillot and M. A. Walker. Unsteady analysis of the air wake over the LPD-17. *AIAA Paper 2000-4125*, 2000.
- [10] M. J. Guillot, M. A. Walker, K. Reader, R. Ramamurti, and W. C. Sandberg. LPD-17 topside aerodynamic study. Final Technical Report, NRL, 2000.
- [11] Y. Kallinderis and A. Chen. An incompressible 3-D Navier-Stokes method with adaptive hybrid grids. *AIAA Paper 1996-0293*, 1996.
- [12] K. J. Karbon and R. Singh. Simulation and design of automobile sunroof buffeting noise control. In *8th AIAA-CEAS Aero-Acoustics Conf.*, Breckenridge, 2002.
- [13] J. Kim and P. Moin. Application of a fractional-step method to incompressible Navier-Stokes equations. *Journal of Computational Physics*, 59:308–323, 1985.
- [14] A. M. Landsberg, J. Boris, W. C. Sandberg, and T. R. Young. Naval ship superstructure design: Complex three-dimensional flows using an efficient parallel method. In *Proc. SCS Simulation Conference*, San Diego, CA, 1993.
- [15] A. M. Landsberg, J. Boris, W. C. Sandberg, and T. R. Young. Analysis of the nonlinear coupling of a helicopter downwash with an unsteady airwake. *AIAA Paper 1995-0047*, 1995.
- [16] A. M. Landsberg and W. C. Sandberg. DDG-51 Flt-IIA Airwake study part 3: Temperature field analysis for baseline and upgrade configuration. Memorandum Report 6401-00-8432, Naval Research Laboratory, Washington, DC, 2000.

- [17] A. M. Landsberg, W. C. Sandberg, T. R. Young, and J. Boris. DDG-51 Flt-IIA Airwake study part 2: Hangar interior flow. Memorandum Report 96-7898, Naval Research Laboratory, Washington, DC, 1996.
- [18] R. Löhner. A fast finite element solver for incompressible flows. *AIAA Paper 1990-0398*, 1990.
- [19] R. Löhner, C. Yang, E. Oñate, and S. Idelsohn. An unstructured grid-based parallel free surface solver. *Applied Numerical Mathematics*, 1999.
- [20] S. A. Polsky. A computational study of unsteady ship airwake. *AIAA Paper 2002-1022*, 2002.
- [21] R. Ramamurti and R. Löhner. A parallel implicit incompressible flow solver using unstructured meshes. *Computers and Fluids*, 5:119–132, 1996.
- [22] R. Ramamurti and W. C. Sandberg. LPD-17 top-side aerodynamic study: FEFLO. NRL Memorandum Report NRL/MR/6410-00-8498, Center for Reactive Flow and Dynamical Systems - Laboratory for Computational Physics and Fluid Dynamics - Naval Research Laboratory, October 2000.
- [23] K. R. Reddy, R. Toffoletto, and K. R. W. Jones. Numerical simulation of ship airwake. *Computers and Fluids*, 29:451–465, 2000.
- [24] A. Sharma and L. N. Long. Airwake simulations on an LPD-17 ship. *AIAA Paper 2001-2589*, 2001.
- [25] J. Smagorinsky. General circulation experiments with the primitive equations. I: The basic experiment. *Monthly Weather Review*, 91:99–165, 1963.